Visualizing the Anomalous Catalysis in Two-Dimensional Confined Space

Zhu-Jun Wang,▲ Zhihua Liang,▲ Xiao Kong,▲ Xiaowen Zhang, Ruixi Qiao, Jinhuan Wang, Shuai Zhang, Zhiqun Zhang, Chaowu Xue, Guoliang Cui, Zhihong Zhang, Dingxin Zou, Zhi Liu, Qunyang Li, Wenya Wei, Xu Zhou, Zhilie Tang, Dapeng Yu, Enge Wang, Kaihui Liu,* Feng Ding,* and Xiaozhi Xu*

ACCESS | Metrics & More | Article Recommendations | Supporting Information

ABSTRACT: Confined nanospaces provide a new platform to promote catalytic reactions. However, the mechanism of catalytic enhancement in the nanospace still requires insightful exploration due to the lack of direct visualization. Here, we report *operando* investigations on the etching and growth of graphene in a two-dimensional (2D) confined space between graphene and a Cu substrate. We observed that the graphene layer between the Cu and top graphene layer was surprisingly very active in etching (more than 10 times faster than the etching of the top graphene layer). More strikingly, at a relatively low temperature (~530 °C), the etched carbon radicals dissociated from the bottom layer, in turn feeding the growth of the top graphene layer with a very high efficiency. Our findings reveal the *in situ* dynamics of the anomalous confined catalytic processes in 2D confined spaces and thus pave the way for the design of high-efficiency catalysts.

KEYWORDS: confined nanospaces, graphene, catalysis, operando observation, in-plan evolution
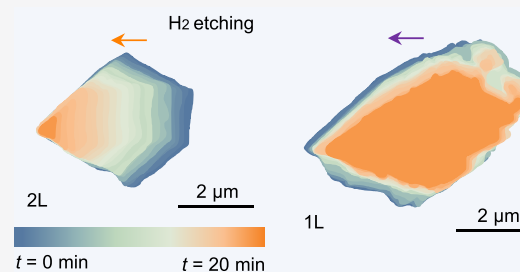
T wo-dimensional (2D) confined space, which is usually composed of 2D material substrates or neighboring 2D materials, possesses atomic-scale gaps, strong matter interactions, and unique nanoenvironments;[1−5] thus, it allows abnormal reactions that cannot take place under normal conditions and has great potential in the applications of materials science and catalysts.[6−21] The 2D confined space could provide an intriguing framework and ultrahigh pressure for stabilizing materials that cannot exist in a traditional atmosphere, which plays a key role in producing novel 2D materials, such as atomically thin ice,[6] GaN,[7] and metals.[8−10] Unlike the case in a conventional open system, in a confined nanospace, the reactants have a large probability to interact with a high electronic density of states, which may lead to high catalytic efficiency. Therefore, 2D confined space has become an intriguing system for the exploration of catalysis with superior activity and stability.[11−14]

To further explore novel 2D materials or high-performance catalysts in confined nanospaces, an investigation and understanding of the real-time and real-space behaviors in 2D confined systems are certainly prerequisites.[22] However, to date, the understanding of confined catalytic processes is still based on feedback from *ex situ* measurements. In principle, the proposed mechanism of catalytic processes that rely on *ex situ* characterizations may be incapable of describing the full picture of the dynamics in confined nanospaces. Therefore, visualizing the actual reaction processes and understanding of

the confinement effect in the field of catalysis by *in situ* studies are urgently needed.

Here, we present a compact study on the etching and growth of graphene in a 2D confined space. By choosing bilayer graphene/Cu as a model system, where the lower graphene layer is strictly confined by the top graphene layer and the metal substrate, we constructed an ideal confined 2D space for *in situ* real-space observation. The visualization of graphene evolution in 2D space revealed that both the etching and growth of graphene in the confined space are distinctly different from those on the open surface of the metal catalyst: (i) the confined graphene layer exhibits a quite high etching rate, approximately 10 times faster than the top graphene layer on the open catalyst surface; (ii) the carbon radicals released during the etching of the confined graphene layer diffuse through the van der Waals gap to the edge of the top graphene layer and then feed the growth of the top graphene layer at a relatively low temperature (~530 °C). Therefore, our work is a rare case where both the product of the reaction and the
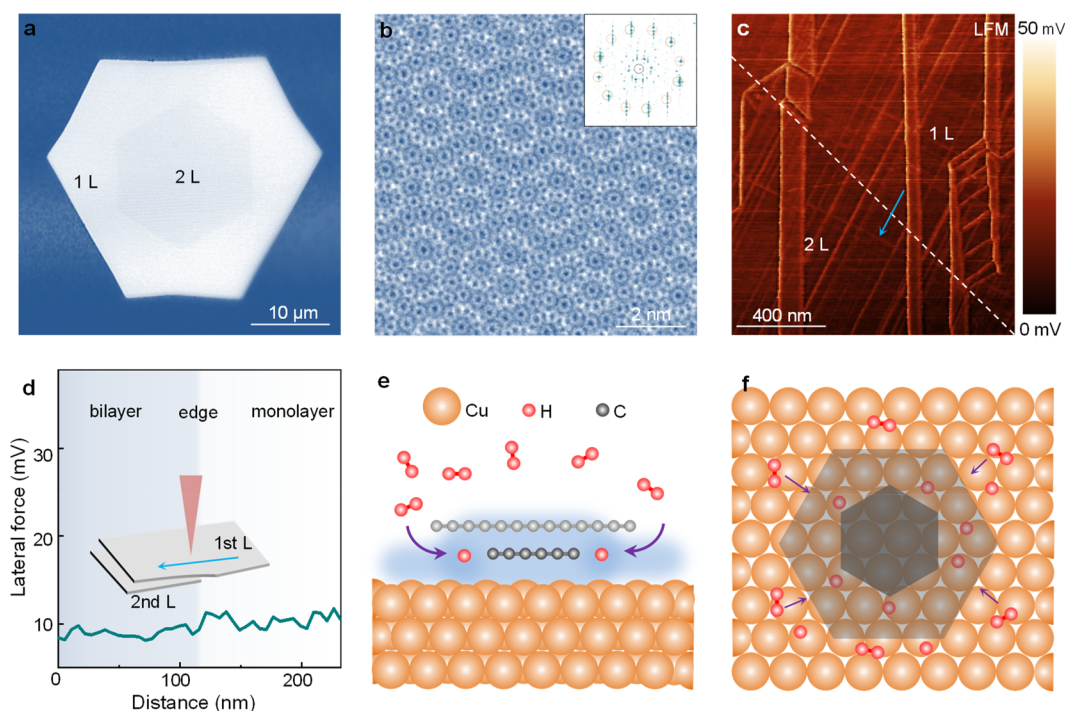
Figure 1. Characterization of bilayer graphene on copper foils. (a) Optical image of a bilayer graphene island. The twist angle is 30°, as identified by the edges. (b) Aberration-corrected transmission electron microscopy image of bilayer graphene. The real-space atomic lattice structure and the reciprocal-space diffraction pattern both indicate that the twist angle is 30°. Inset: fast Fourier transformation patterns of (b). (c, d) Lateral force microscopy image of bilayer graphene. The lateral force profile shows negligible changes in friction when the tip moves from the monolayer to the bilayer graphene area, which proves that the second layer of graphene is grown under the first layer. (e, f) Schematic diagrams of the etching of bilayer graphene in a 2D confined system.

dynamics of product evolution can be directly observed. Our findings clearly reveal that the catalytic reaction in a 2D confined space is highly different from that in an open space and that the mass transport in the confined space plays a central role in bridging the catalytic etching of the bottom-layer graphene and the catalytic growth of the top-layer graphene. We expect this study to facilitate the design of catalytic systems in a confined space for various applications.

In our experiment, bilayer graphene samples were synthesized by a heat-resisting-box-assisted chemical vapor deposition (CVD) method to remove the particles on graphene surface (see Methods for details).[23] The bilayer graphene samples and their twist angles can be directly identified with optical microscopy on the basis of the different optical contrasts (Figure 1a). In addition to optical identification, the twist angle between two graphene layers was further confirmed by aberration-corrected transmission electron microscopy (TEM). The real-space atomic lattice structure and the reciprocal-space diffraction pattern both indicate that the twist angle is 30° (Figure 1b). To confirm whether the second graphene layer was above or underneath the first graphene layer, we conducted friction force microscopy measurements (Figure 1c). For a bilayer graphene where the second layer is on the top, the edge of the second-layer graphene will be exposed and the carbon atoms have been reported to be mainly determined with hydroxyl (C−OH) and alkyl (C−H) groups.[24] When the AFM tip moves across the edge, the friction forces will be obviously enhanced, resulting in a sharp peak in the lateral force profile (Figure S1). For a bilayer graphene where the second layer is at the bottom, the edge of the second layer graphene is buried and there would be no obvious changes in fraction force at the edge

(Figure S1). The lateral force profile shows negligible changes in friction when the tip moves from the monolayer to the bilayer graphene area (Figure 1d), which strongly proves that the second graphene layer is grown under the first layer. Then, we can construct an ideal 2D confined system and analyze the unique reaction behaviors in it by *operando* monitoring the growth and etching behaviors of the lower and top graphene layers under a near-ambient-pressure atmosphere (schematic diagrams are shown in Figure 1e,f).

We first analyzed the etching behavior of the bilayer graphene samples under a hydrogen atmosphere. At the beginning, etching of graphene occurred at the wrinkles (Figure S2). The behaviors at this stage were neglected because they are affected by surface topography, which did not reflect the intrinsic etching behaviors in 2D confined systems. After all of the wrinkles were etched, we *operando* recorded the evolution of the top large and lower small graphene layers over time and found completely unexpected etching behaviors. As the lower graphene layer is restricted by the top layer and the Cu substrate, where the interfacial space allowing hydrogen atom diffusion is only at the sub-nanometer scale, one would intuitively think it is very hard to etch the lower graphene layer. However, an exceptionally high etching rate was observed (Figure 2a−f and Movie S1). In contrast, although the top graphene layer was completely exposed to hydrogen, the etching was very slow (Figure 2a−f and Movie S1).

To quantitatively study the etching rates of the top and lower graphene layers, we performed a statistical analysis of the graphene islands at different times and calculated their etching rates along the horizontal direction, indicated by the arrows in Figure 2g,h. The results show that the etching rate of the restricted lower graphene layer is approximately 0.2 μm/min,
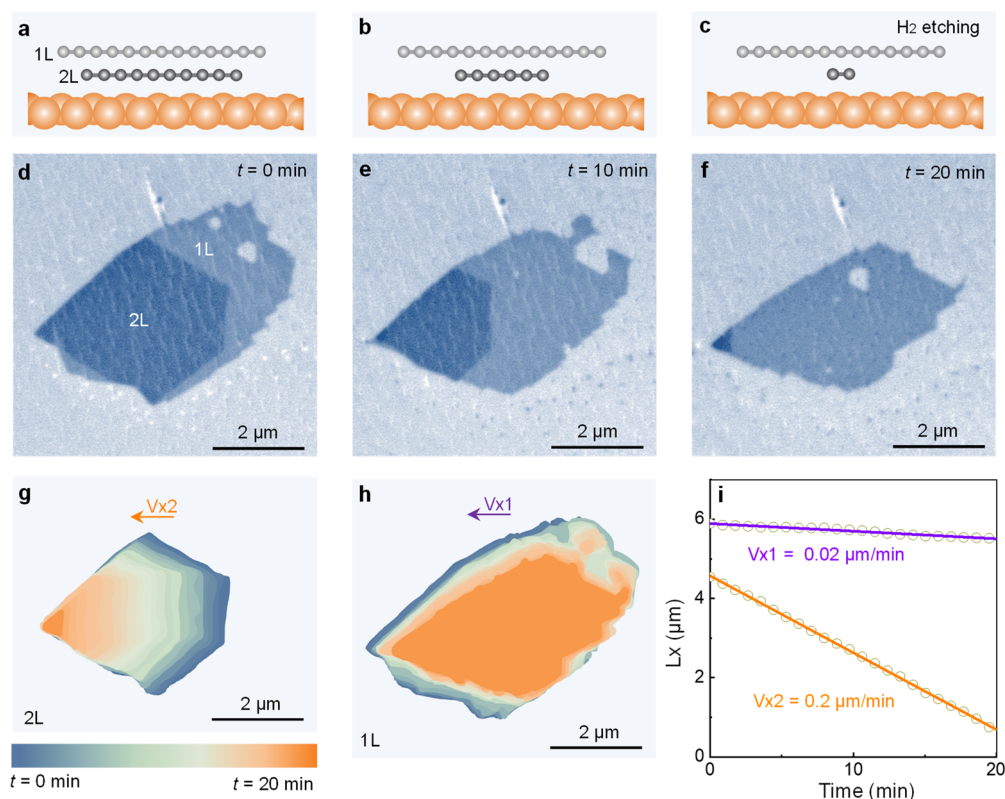
Figure 2. Etching behavior of the top and lower graphene layers. (a−c) Schematic diagrams of the etching process of bilayer graphene in a confined system. (d−f) *In situ* SEM images of bilayer graphene during H_2 etching at different times at 834 °C. The lower graphene layer is etched much more quickly than the top layer. (g, h) Shape evolution of the lower (g) and top (h) graphene islands during H_2 etching. The different colors correspond to different times. (i) Plot and fit of the size of the lower graphene layer (dark yellow circles and orange line) and the top graphene layer (dark yellow circles and violet line) along the horizontal direction as a function of time. The etching rate of the restricted lower graphene layer is 0.2 μm/min, approximately 10 times higher than that of the exposed top layer.
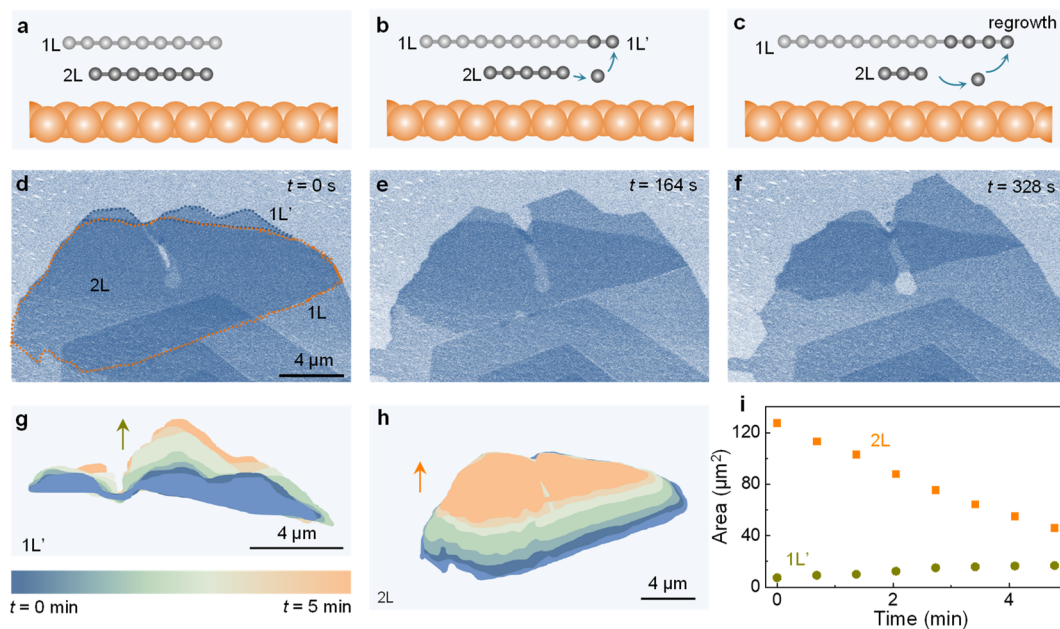
Figure 3. Growth behavior of the top graphene layer. (a−c) Schematic diagrams of the etching and growth process of bilayer graphene in a confined system. (d−f) *In situ* SEM images of bilayer graphene during H_2 etching at different times at 530 °C. The lower graphene layer is etched (marked 2L), but the top graphene layer grows larger (marked 1L′). (g, h) Shape evolution of the top (g) and lower (h) graphene islands during H_2 etching. The different colors correspond to different times. (i) Plot of the area of the lower graphene layer (orange square) and the top graphene layer (dark yellow circles) as a function of time. The area of the lower graphene layer keeps decreasing, but the area of the top graphene layer keeps increasing. The increased area of the top graphene layer was approximately 12% of the decreased area of the lower layer.
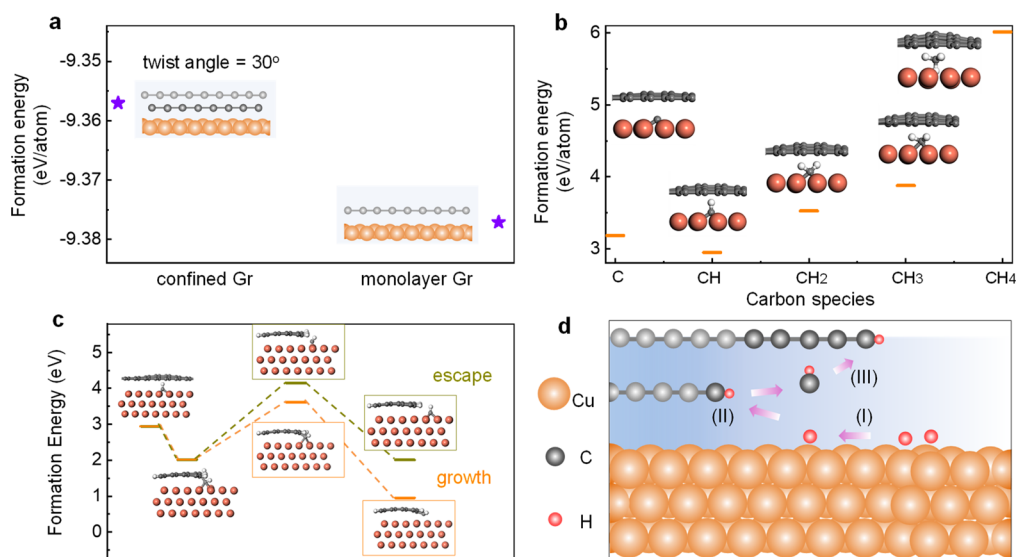
Figure 4. Theoretical understanding of the etching and growth behaviors of graphene in 2D confined space. (a) Formation energies of bilayer graphene/Cu and monolayer graphene/Cu in a confined system. The formation energy of bilayer graphene on the Cu(111) surface is ∼20 meV per carbon atom higher than that of monolayer graphene. Thus, the evolution from bilayer graphene to monolayer graphene is energetically favorable. (b) Formation energies of different hydrocarbon atoms, molecules, and radicals on the Cu surface beneath a graphene layer. The most energy favorable hydrocarbon is the CH radical. (c) Energy profile for CH at different positions during the top layer graphene growth (dark yellow) and the escape process (orange). The growth process has a lower barrier and the reaction kinetics are highly exothermic, ensuring that the growth of top-layer graphene is both thermodynamically and kinetically favorable. (d) Schematic diagram of the etching of the lower graphene layer and growth of the top graphene layer via the diffusion of released radicals through the 2D confined space.

10 times higher than that of the top graphene layer (Figure 2i). Our findings demonstrated that the catalytic etching process in a 2D confined space is completely different from that in open systems and that the unique nanoenvironment in the confined space leads to great changes in the catalytic reactions, which may help to understand the abnormal catalytic behaviors in various confined systems.

In addition to this abnormal etching behavior, further *operando* detections also found abnormal growth behaviors of graphene in the 2D confined system. Under a hydrogen atmosphere, the lower graphene layer was rapidly etched away, while the top layer was not etched but grew larger without introducing any carbon source (the lowest tolerable temperature was ∼530 °C). It seems that the lower graphene layer has been transformed into the top layer through the 2D confined space (Figure 3a−f and Movie S2). To analyze this transformation in detail, we also detected the area evolution of the top and lower graphene layers over time. As time elapses, the area of the lower confined graphene becomes increasingly smaller, while the top graphene grows increasingly larger (Figure 3g,h). A quantitative analysis shows that the increased area of the top graphene layer is approximately 12% of the decreased area of the lower graphene layer (Figure 3i). Therefore, we can preliminarily assume that, after etching of the lower graphene layer, etched carbon species diffuse through the van der Waals gap and attach to the edge of the top graphene layer, leading to the consequent growth of the top graphene layer. Obviously, due to the existence of the 2D confined space, the etching and growth behaviors of graphene are both greatly changed in comparison with those under normal conditions.

To further explore the underlying mechanism, we then carried out first-principles calculations. We first compared the formation energy of bilayer graphene and monolayer graphene on Cu and found that the formation energy for the bilayer was ∼20 meV per atom higher than that for the monolayer (Figure 4a and see Figure S3 for the calculation details). Due to this energy difference, the bilayer graphene tends to be a single layer by etching of one layer and/or the growth of another layer. The etching mechanisms of the top and lower layers must be different. To find out which layer was etched in our experiments, we considered two models of etching: (i) etching of the upper layer graphene would result in carbon species being released into the gas-phase environment and thus it could not support the growth of the lower layer; (ii) in contrast, if the lower layer graphene was etched, the etched carbon species could diffuse to the edge of upper layer graphene and attach to it, which will lead to the growth of the upper edge. On the basis of the experimental observations, we chose the second model in our study. Then, we calculated the energy changes of removing one carbon atom from the edges of lower layer and upper layer graphene, respectively. The results revealed that the etching of the restricted lower graphene layer was ∼110 meV lower than that of the top layer (Figure S4). Therefore, due to the unique confined structure, catalytic etching is greatly promoted.

As was mentioned above, during the etching of the lower graphene layer, the top graphene layer would grow without an external carbon source supply. One possibility is that the confined hydrocarbons diffuse through the interfacial gap and feed the growth of the top graphene layer. To confirm the type of hydrocarbons, we calculated the chemical potential of hydrogen under the experimental conditions, where $\mu_H = -0.97$ eV at $T = 900$ K and $P_{H_2} = 10^{-4}$ bar (Figure S5a). In previous reports, Wu et al. found that the carbon dimer is stable without hydrogen.[25] However, Shu et al. showed that CH_x are the dominating species in graphene growth in the presence of hydrogen.[26] Here, we consider CH_x hydrocarbons on the basis of the experimental condition of graphene etching. In comparison with the diagram of CH_x hydrocarbons (Figure

S5b), we can conclude that the dominant hydrocarbons under our conditions are CH (Figure 4b and see Figure S6 for the calculation details). The calculated in-plane diffusion barrier of CH in the small gap between graphene and Cu(111) is only 0.6 eV (Figure S5c), which corresponds to a diffusion coefficient of $D = \frac{k_{\mathrm{B}} T a_0^2}{4h} \exp\left(-\frac{E_b}{k_{\mathrm{B}} T}\right) \approx 1.30 \times 10^7 \ \mu\mathrm{m}^2 \, \mathrm{s}^{-1}$. On this basis, we can estimate that a CH group could diffuse $\sim 2\sqrt{Dt} \approx 3.6$ mm in 1 s, which is more than 1000 times larger than the distance between the two graphene edges and thus every CH released by the lower graphene layer can quickly react with the edge of the upper graphene layer. When the CH groups pass the edge of the upper layer, they may be captured by the edge carbon atoms (Figure S7b) or directly diffuse out (Figure S7e,f). Once they were captured, our calculations show that the growth process has a lower barrier than that of escape and that the reaction is highly exothermic, which proves that the growth of the top graphene layer is both thermodynamically and kinetically favorable (Figure 4c and see Figure S7 for the calculation details). Due to the continuous CH supply, the growth temperature of the top graphene layer can be as low as 530 °C in our experiment, which is much lower than the traditional graphene growth process on Cu, as it does not need additional energy to decompose methane.[27] It is worth noting that, in these catalytic etching and growth processes, graphene served as both the reactant and product, which is quite unique and hard to directly observe in catalysis.

Then, we can have a clear picture of the abnormal etching and growth processes in the 2D confined space. Under a hydrogen atmosphere, hydrogen first diffuses onto the Cu substrate, terminates at the graphene edges, and then starts to etch the graphene. Due to the different formation energies, the restricted lower graphene layer would be etched more quickly than the top layer. The fast etching and small diffusion barrier guarantee sufficient CH groups in the small gap, which in turn feed the growth of the top graphene layer, as it is both thermodynamically and kinetically favorable (Figure 4d). Our findings clearly reveal the anomalous reaction behaviors in 2D confined space and offer a new opportunity for the design of high-efficiency catalysts in the future.

■ METHODS

Growth of Bilayer Graphene Samples. Bilayer graphene was grown by using a chemical vapor deposition (CVD) method. The Cu foils (25 μm thick, 99.8%, Alfa Aesar) were directly used without pretreatment. The Cu foils were put into a self-designed heat-resistant box, and then they were loaded into a quartz tube with a diameter of 5.5 cm. The heat-resistant box was used to keep SiO_2 particles from shedding from the quartz tube on the Cu surface, providing clean and high-quality graphene samples (Figure S8a,b). Otherwise, the H_2 etching would always start from the particles and could not reflect the intrinsic etching behaviors of graphene (Figure S8c). In the growth process, we added some graphite powder in the box; it was used as a kind of solid carbon source to increase the bilayer growth on Cu, as industrial graphite usually contains polyaromatic hydrocarbons that can be released at high temperature. The furnace was heated to 1030 °C under an Ar atmosphere (500 sccm) for 1 h and then annealed with H_2 (5 sccm) for 40 min. After the annealing, CH_4 (2 sccm) was introduced as the carbon source for graphene growth. Finally, the furnace was cooled naturally with Ar (1000 sccm).

In Situ Observations by Environmental SEM. *In situ* etching of graphene samples was performed inside the chamber of a modified environmental SEM system (Thermo Fisher Quattro ESEM) with a custom infrared laser heating stage and with gas supplied through a leak valve. The etching temperature ranged from 530 to 900 °C under 140 Pa. Images were recorded by a large-field detector during etching. During the experiments, the microscope was operated at an acceleration voltage of 5.0−7.5 kV. No influence of the electron beam on the growth and etching process could be observed.[28,29] The imaged regions and their respective surroundings showed similar behaviors, as evidenced by changing the magnification or by moving the sample under the beam. Furthermore, no electron-beam-induced contamination was observed at elevated temperatures.

Characterization. AFM measurements were performed using an Asylum Research Cypher instrument under ambient conditions. Optical images of graphene were taken with an Olympus microscope (Olympus BX51). The graphene sample for TEM characterization was prepared by transferring graphene onto commercial holey-carbon TEM grids (Zhongjingkeyi GIG-2010-3C) using the polymethyl methacrylate based transfer technique. STEM experiments were performed with a FEI Titan Themis G2 300 instrument operated at 80 kV.

Computational Details. The Vienna *ab initio* simulation package (VASP) was employed for DFT calculations.[30,31] The Perdew−Burke−Ernzerhof parametrization of generalized gradient approximation (GGA) was used for the exchange-correlation function.[32] The ion−electron interactions were embodied in a projector augmented wave method with a cutoff energy of 400 eV.[33] The Grimme DFT-D3 (BJ) method was used for the corrections of the interlayer van der Waals interaction.[34,35] The electronic self-consistency criterion was set to 10^{-4} eV. For geometry relaxation, the force on atoms was converged below 0.01 eV Å^{-1}. The energy barriers were calculated by using the climbing image nudged elastic band (CI-NEB) method[36] with a force threshold of 0.01 eV Å^{-1}. To avoid interference of the image, a vacuum slab of 20 Å perpendicular to the graphene plane was used for all calculations. The Cu(111) substrate in all calculation models is slightly compressed to match the lattice of graphene. The substrate contains four layers of Cu, where the bottom layer is fixed to mimic the bulk Cu.

The formation energy of monolayer (bilayer) graphene on Cu(111) surface is calculated by $E_f = \frac{E_{\mathrm{G/Cu}} - E_{\mathrm{Cu}}}{N_C}$, where $E_{\mathrm{G/Cu}}$ is the total energy of monolayer (bilayer) graphene on Cu and E_{Cu} is the energy of the substrate. The bottom layer of graphene is rotated by 28°, constructing a commeasurable supercell with 26 C atoms in each layer (Figure S3). Then the models were sampled by a $3 \times 3 \times 1$ k-mesh using the Monkhorst−Pack method.[37]

To calculate the formation energy of hydrocarbons, each hydrocarbon molecule was confined in a 7×7 superlattice of monolayer graphene on Cu(111), and the model was sampled by a $1 \times 1 \times 1$ k-mesh. The formation energy of the hydrocarbon was $E_{\mathrm{CH}_n} = E_{\mathrm{G/CH}_n/\mathrm{Cu}} - E_{\mathrm{G/Cu}} - E_{\mathrm{fm}} - n(E_{\mathrm{H}_2}/2 + \mu_{\mathrm{H}})$, where $E_{\mathrm{G/CH}_n/\mathrm{Cu}}$ is the total energy of the model, $E_{\mathrm{G/Cu}}$ is the energy of monolayer graphene on Cu, E_{fm} is the formation energy of one carbon in the monolayer graphene on Cu, E_{H_2} is the energy of a hydrogen molecule, and μ_{H} is the chemical

potential of H. The formation energy of CH at the edge or on the exposed substrate is $E_{CH} = E_{CH@site} - E_{ref} - E_{fm} - n(E_{H_2}/2 + \mu_H)$, where $E_{CH@site}$ is the total model of CH attached to the edge or on the exposed substrate and E_{ref} is the energy of that model without CH. All of the models are shown in Figure S7.

■ ASSOCIATED CONTENT

ⓈⒾ Supporting Information

The Supporting Information is available free of charge at https://pubs.acs.org/doi/10.1021/acs.nanolett.2c00549.

> AFM characterizations of bilayer graphene, shape evolution of the bilayer graphene during etching, DFT calculation models of monolayer/bilayer graphene on Cu(111) surface, theoretical calculations of the etching of upper and lower graphene layers, hydrogens in the confined space, DFT calculation models of hydrocarbons in the confined space, DFT calculation models of CH at different sites, and characterization of graphene produced with and without the heat-resistant box (PDF)

> shape evolution of the bilayer graphene islands during H_2 etching (AVI)

> shape evolution of the bilayer graphene islands during regrowth (AVI)

■ AUTHOR INFORMATION

Corresponding Authors

Kaihui Liu − *State Key Laboratory for Mesoscopic Physics, Frontiers Science Center for Nano-optoelectronics, School of Physics, Peking University, Beijing 100871, People's Republic of China; International Centre for Quantum Materials, Collaborative Innovation Centre of Quantum Matter, Peking University, Beijing 100871, People's Republic of China;* ⓞ orcid.org/0000-0002-8781-2495; Email: khliu@pku.edu.cn

Feng Ding − *Centre for Multidimensional Carbon Materials, Institute for Basic Science, Ulsan 44919, South Korea; School of Materials Science and Engineering, Ulsan National Institute of Science and Technology, Ulsan 44919, South Korea;* ⓞ orcid.org/0000-0001-9153-9279; Email: f.ding@unist.ac.kr

Xiaozhi Xu − *Guangdong Provincial Key Laboratory of Quantum Engineering and Quantum Materials, School of Physics and Telecommunication Engineering, South China Normal University, Guangzhou 510631, People's Republic of China; Guangdong-Hong Kong Joint Laboratory of Quantum Matter, South China Normal University, Guangzhou 510631, People's Republic of China;* ⓞ orcid.org/0000-0003-1067-9590; Email: xiaozhixu@scnu.edu.cn

Authors

Zhu-Jun Wang − *Guangdong Provincial Key Laboratory of Quantum Engineering and Quantum Materials, School of Physics and Telecommunication Engineering, South China Normal University, Guangzhou 510631, People's Republic of China; Guangdong-Hong Kong Joint Laboratory of Quantum Matter, South China Normal University, Guangzhou 510631, People's Republic of China; School of Physical Science and Technology, Shanghai Tech University, Shanghai 201210, People's Republic of China;* ⓞ orcid.org/0000-0002-8227-7323

Zhihua Liang − *Guangdong Provincial Key Laboratory of Quantum Engineering and Quantum Materials, School of Physics and Telecommunication Engineering, South China Normal University, Guangzhou 510631, People's Republic of China; Guangdong-Hong Kong Joint Laboratory of Quantum Matter, South China Normal University, Guangzhou 510631, People's Republic of China*

Xiao Kong − *Centre for Multidimensional Carbon Materials, Institute for Basic Science, Ulsan 44919, South Korea*

Xiaowen Zhang − *Guangdong Provincial Key Laboratory of Quantum Engineering and Quantum Materials, School of Physics and Telecommunication Engineering, South China Normal University, Guangzhou 510631, People's Republic of China; Guangdong-Hong Kong Joint Laboratory of Quantum Matter, South China Normal University, Guangzhou 510631, People's Republic of China*

Ruixi Qiao − *State Key Laboratory for Mesoscopic Physics, Frontiers Science Center for Nano-optoelectronics, School of Physics, Peking University, Beijing 100871, People's Republic of China; International Centre for Quantum Materials, Collaborative Innovation Centre of Quantum Matter, Peking University, Beijing 100871, People's Republic of China*

Jinhuan Wang − *State Key Laboratory for Mesoscopic Physics, Frontiers Science Center for Nano-optoelectronics, School of Physics, Peking University, Beijing 100871, People's Republic of China;* ⓞ orcid.org/0000-0001-5569-8520

Shuai Zhang − *Department of Engineering Mechanics, State Key Laboratory of Tribology, Tsinghua University, Beijing 100084, People's Republic of China*

Zhiqun Zhang − *School of Physical Science and Technology, Shanghai Tech University, Shanghai 201210, People's Republic of China*

Chaowu Xue − *School of Physical Science and Technology, Shanghai Tech University, Shanghai 201210, People's Republic of China*

Guoliang Cui − *Guangdong Provincial Key Laboratory of Quantum Engineering and Quantum Materials, School of Physics and Telecommunication Engineering, South China Normal University, Guangzhou 510631, People's Republic of China; Guangdong-Hong Kong Joint Laboratory of Quantum Matter, South China Normal University, Guangzhou 510631, People's Republic of China*

Zhihong Zhang − *Beijing Advanced Innovation Center for Materials Genome Engineering, Institute for Multidisciplinary Innovation, University of Science and Technology Beijing, Beijing 100083, People's Republic of China*

Dingxin Zou − *Shenzhen Institute for Quantum Science and Engineering, Southern University of Science and Technology, Shenzhen 518055, People's Republic of China*

Zhi Liu − *School of Physical Science and Technology, Shanghai Tech University, Shanghai 201210, People's Republic of China;* ⓞ orcid.org/0000-0002-8973-6561

Qunyang Li − *Department of Engineering Mechanics, State Key Laboratory of Tribology, Tsinghua University, Beijing 100084, People's Republic of China;* ⓞ orcid.org/0000-0002-6865-3863

Wenya Wei − *Guangdong Provincial Key Laboratory of Quantum Engineering and Quantum Materials, School of Physics and Telecommunication Engineering, South China Normal University, Guangzhou 510631, People's Republic of China; Guangdong-Hong Kong Joint Laboratory of Quantum Matter, South China Normal University, Guangzhou 510631, People's Republic of China*

Xu Zhou − *Guangdong Provincial Key Laboratory of Quantum Engineering and Quantum Materials, School of Physics and Telecommunication Engineering, South China Normal University, Guangzhou 510631, People's Republic of China; Guangdong-Hong Kong Joint Laboratory of Quantum Matter, South China Normal University, Guangzhou 510631, People's Republic of China*

Zhilie Tang − *Guangdong Provincial Key Laboratory of Quantum Engineering and Quantum Materials, School of Physics and Telecommunication Engineering, South China Normal University, Guangzhou 510631, People's Republic of China; Guangdong-Hong Kong Joint Laboratory of Quantum Matter, South China Normal University, Guangzhou 510631, People's Republic of China*

Dapeng Yu − *Shenzhen Institute for Quantum Science and Engineering, Southern University of Science and Technology, Shenzhen 518055, People's Republic of China*

Enge Wang − *International Centre for Quantum Materials, Collaborative Innovation Centre of Quantum Matter, Peking University, Beijing 100871, People's Republic of China; Songshan Lake Materials Laboratory, Institute of Physics, Chinese Academy of Sciences, Dongguan, Guangdong 523808, People's Republic of China; School of Physics, Liaoning University, Shenyang 110036, China*

Complete contact information is available at:
https://pubs.acs.org/10.1021/acs.nanolett.2c00549

Author Contributions

▲Z.-J.W., Z.L., and X.K. contributed equally to this work.

Author Contributions

X.X. and Z.-J.W. conceived of the project. Z.L., X.Z., Z.Z., G.C., and D.Z. performed the graphene growth. Z.-J.W. modified the environmental SEM. Z.Z., C.X., Z.L., and Z.-J.W. performed the *in situ* SEM measurements. X.K. and F.D. performed the DFT calculations. R.Q. and D.Y. performed the TEM measurements. J.W., S.Z. and Q.L. conducted the AFM measurements. W.W., X.Z., Z.T., E.W., K.L., and X.X. analyzed and discussed the data.

Notes

The authors declare no competing financial interest.

■ REFERENCES

(1) Fu, Q.; Bao, X. H. Confined microenvironment for catalysis control. *Nat. Catal* **2019**, *2*, 834−836.

(2) Woessner, A.; Lundeberg, M. B.; Gao, Y.; Principi, A.; Alonso-Gonzalez, P.; Carrega, M.; Watanabe, K.; Taniguchi, T.; Vignale, G.; Polini, M.; Hone, J.; Hillenbrand, R.; Koppens, F. H. L.; et al. Highly confined low-loss plasmons in graphene-boron nitride heterostructures. *Nat. Mater.* **2015**, *14*, 421−425.

(3) Alcaraz Iranzo, D.; Nanot, S.; Dias, E. J. C.; Epstein, I.; Peng, C.; Efetov, D. K.; Lundeberg, M. B.; Parret, R.; Osmond, J.; Hong, J.-Y.; Kong, J.; Englund, D. R.; Peres, N. M. R.; Koppens, F. H. L.; et al. Probing the ultimate plasmon confinement limits with a van der Waals heterostructure. *Science* **2018**, *360*, 291−295.

(4) Vasu, K. S.; Prestat, E.; Abraham, J.; Dix, J.; Kashtiban, R. J.; Beheshtian, J.; Sloan, J.; Carbone, P.; Neek-Amal, M.; Haigh, S. J.; et al. Van der Waals pressure and its effect on trapped interlayer molecules. *Nat. Commun.* **2016**, *7*, 12168.

(5) Khestanova, E.; Guinea, F.; Fumagalli, L.; Geim, A. K.; Grigorieva, I. V. Universal shape and pressure inside bubbles appearing in van der Waals heterostructures. *Nat. Commun.* **2016**, *7*, 12587.

(6) Algara-Siller, G.; Lehtinen, O.; Wang, F. C.; Nair, R. R.; Kaiser, U.; Wu, H. A.; Geim, A. K.; Grigorieva, I. V. Square ice in graphene nanocapillaries. *Nature* **2015**, *519*, 443−445.

(7) Al Balushi, Z. Y.; Wang, K.; Ghosh, R. K.; Vila, R. A.; Eichfeld, S. M.; Caldwell, J. D.; Qin, X. Y.; Lin, Y. C.; DeSario, P. A.; Stone, G.; et al. Two-dimensional gallium nitride realized via graphene encapsulation. *Nat. Mater.* **2016**, *15*, 1166−1171.

(8) Huang, X.; Li, S. Z.; Huang, Y. Z.; Wu, S. X.; Zhou, X. Z.; Li, S. Z.; Gan, C. L.; Boey, F.; Mirkin, C. A.; Zhang, H. Synthesis of hexagonal close-packed gold nanostructures. *Nat. Commun.* **2011**, *2*, 292.

(9) Wang, L.; Zhu, Y. H.; Wang, J. Q.; Liu, F. D.; Huang, J. F.; Meng, X. J.; Basset, J. M.; Han, Y.; Xiao, F. S. Two-dimensional gold nanostructures with high activity for selective oxidation of carbon-hydrogen bonds. *Nat. Commun.* **2015**, *6*, 6957.

(10) Briggs, N.; Bersch, B.; Wang, Y. X.; Jiang, J.; Koch, R. J.; Nayir, N.; Wang, K.; Kolmer, M.; Ko, W.; Duran, A. D.; et al. Atomically thin half-van der Waals metals enabled by confinement heteroepitaxy. *Nat. Mater.* **2020**, *19*, 637−643.

(11) Deng, D. H.; Novoselov, K. S.; Fu, Q.; Zheng, N. F.; Tian, Z. Q.; Bao, X. H. Catalysis with two-dimensional materials and their heterostructures. *Nat. Nanotechnol* **2016**, *11*, 218−230.

(12) Shifa, T. A.; Vomiero, A. Confined Catalysis: Progress and Prospects in Energy Conversion. *Adv. Energy Mater.* **2019**, *9*, 1902307.

(13) Tang, L.; Meng, X. G.; Deng, D. H.; Bao, X. H. Confinement Catalysis with 2D Materials for Energy Conversion. *Adv. Mater.* **2019**, *31*, 1901996.

(14) Li, Z. H.; Zhang, X.; Cheng, H. F.; Liu, J. W.; Shao, M. F.; Wei, M.; Evans, D. G.; Zhang, H.; Duan, X. Confined Synthesis of 2D Nanostructured Materials toward Electrocatalysis. *Adv. Energy Mater.* **2020**, *10*, 1900486.

(15) Merlet, C.; Pean, C.; Rotenberg, B.; Madden, P. A.; Daffos, B.; Taberna, P. L.; Simon, P.; Salanne, M. Highly confined ions store charge more efficiently in supercapacitors. *Nat. Commun.* **2013**, *4*, 2701.

(16) Moeremans, B.; Cheng, H. W.; Hu, Q. Y.; Garces, H. F.; Padture, N. P.; Renner, F. U.; Valtiner, M. Lithium-ion battery electrolyte mobility at nano-confined graphene interfaces. *Nat. Commun.* **2016**, *7*, 12693.

(17) Voiry, D.; Fullon, R.; Yang, J. E.; Silva, C. D. C. E.; Kappera, R.; Bozkurt, I.; Kaplan, D.; Lagos, M. J.; Batson, P. E.; Gupta, G.; et al. The role of electronic coupling between substrate and 2D MoS2 nanosheets in electrocatalytic production of hydrogen. *Nat. Mater.* **2016**, *15*, 1003−1009.

(18) Fu, Q.; Bao, X. H. Surface chemistry and catalysis confined under two-dimensional materials. *Chem. Soc. Rev.* **2017**, *46*, 1842−1874.

(19) Li, H. B.; Xiao, J. P.; Fu, Q.; Bao, X. H. Confined catalysis under two-dimensional materials. *P Natl. Acad. Sci. USA* **2017**, *114*, 5930−5934.

(20) Pis, I.; Magnano, E.; Nappini, S.; Bondino, F. Under-cover stabilization and reactivity of a dense carbon monoxide layer on Pt(111). *Chem. Sci.* **2019**, *10*, 1857−1865.

(21) Riscoe, A. R.; Wrasman, C. J.; Herzing, A. A.; Hoffman, A. S.; Menon, A.; Boubnov, A.; Vargas, M.; Bare, S. R.; Cargnello, M. Transition state and product diffusion control by polymer-nanocrystal hybrid catalysts. *Nat. Catal* **2019**, *2*, 852−863.

(22) Barroo, C.; Wang, Z.-J.; Schlögl, R.; Willinger, M.-G. Imaging the dynamics of catalysed surface reactions by in situ scanning electron microscopy. *Nat. Catal* **2020**, *3*, 30−39.

(23) Xu, X. Z.; Qiao, R. X.; Liang, Z. H.; Zhang, Z. H.; Wang, R.; Zeng, F. K.; Cui, G. L.; Zhang, X. W.; Zou, D. X.; Guo, Y.; et al. Towards intrinsically pure graphene grown on copper. *Nano Res.* **2021**, *14*, 4878−4884.

(24) Chen, Z.; Khajeh, A.; Martini, A.; Kim, S. H. Chemical and physical origins of friction on surfaces with atomic steps. *Sci. Adv.* **2019**, *5*, No. eaaw0513.

(25) Wu, P.; Zhang, Y.; Cui, P.; Li, Z. Y.; Yang, J. L.; Zhang, Z. Y. Carbon Dimers as the Dominant Feeding Species in Epitaxial Growth and Morphological Phase Transition of Graphene on Different Cu Substrates. *Phys. Rev. Lett.* **2015**, *114*, 216102.

(26) Shu, H. B.; Tao, X. M.; Ding, F. What are the active carbon species during graphene chemical vapor deposition growth? *Nanoscale* **2015**, *7*, 1627−1634.

(27) Li, X. S.; Cai, W. W.; An, J. H.; Kim, S.; Nah, J.; Yang, D. X.; Piner, R.; Velamakanni, A.; Jung, I.; Tutuc, E.; et al. Large-Area Synthesis of High-Quality and Uniform Graphene Films on Copper Foils. *Science* **2009**, *324*, 1312−1314.

(28) Wang, Z. J.; Weinberg, G.; Zhang, Q.; Lunkenbein, T.; Klein-Hoffmann, A.; Kurnatowska, M.; Plodinec, M.; Li, Q.; Chi, L. F.; Schloegl, R.; et al. Direct Observation of Graphene Growth and Associated Copper Substrate Dynamics by in Situ Scanning Electron Microscopy. *ACS Nano* **2015**, *9*, 1506−1519.

(29) Wang, Z. J.; Dong, J. C.; Cui, Y.; Eres, G.; Timpe, O.; Fu, Q.; Ding, F.; Schloegl, R.; Willinger, M. G. Stacking sequence and interlayer coupling in few-layer graphene revealed by in situ imaging. *Nat. Commun.* **2016**, *7*, 13256.

(30) Kresse, G.; Furthmuller, J. Efficiency of ab-initio total energy calculations for metals and semiconductors using a plane-wave basis set. *Comput. Mater. Sci.* **1996**, *6*, 15−50.

(31) Kresse, G.; Furthmuller, J. Efficient iterative schemes for ab initio total-energy calculations using a plane-wave basis set. *Phys. Rev. B* **1996**, *54*, 11169−11186.

(32) Perdew, J. P.; Burke, K.; Ernzerhof, M. Generalized gradient approximation made simple. *Phys. Rev. Lett.* **1996**, *77*, 3865−3868.

(33) Kresse, G.; Joubert, D. From ultrasoft pseudopotentials to the projector augmented-wave method. *Phys. Rev. B* **1999**, *59*, 1758−1775.

(34) Grimme, S.; Antony, J.; Ehrlich, S.; Krieg, H. A consistent and accurate ab initio parametrization of density functional dispersion correction (DFT-D) for the 94 elements H-Pu. *J. Chem. Phys.* **2010**, *132*, 154104.

(35) Grimme, S.; Ehrlich, S.; Goerigk, L. Effect of the Damping Function in Dispersion Corrected Density Functional Theory. *J. Comput. Chem.* **2011**, *32*, 1456−1465.

(36) Henkelman, G.; Uberuaga, B. P.; Jonsson, H. A climbing image nudged elastic band method for finding saddle points and minimum energy paths. *J. Chem. Phys.* **2000**, *113*, 9901−9904.

(37) Monkhorst, H. J.; Pack, J. D. Special points for Brillouin-zone integrations. *Phys. Rev. B* **1976**, *13*, 5188−5192.